Texila International Journal of Public Health
Special Issue-1 2024
DOI: 10.21522/TIJPH.2013.SE.24.01.Art005

Microwave-Assisted Hydrothermal Synthesis of Ru-doped Mn_3O_4 Nanoflowers for Biomedical Applications

Hooriyah Laiq Ahmed Khan[1], Vishnu Priya Veeraraghavan[2*], Pitchaimani Veerakumar[2*]
[1]*Saveetha Dental College and Hospitals, Saveetha Institute of Medical and Technical Sciences, Saveetha University, Chennai*
[2]*Centre of Molecular Medicine and Diagnostics, Department of Biochemistry, Saveetha Dental College and Hospitals, Saveetha Institute of Medical and Technical Sciences, Saveetha University, Chennai*

Abstract

Ruthenium-doped manganese oxide nanoflowers (denoted as Ru-Mn3O4 NFs) were synthesized via microwave-assisted hydrothermal (MW-HT) method. The prepared NFs were evaluated for antimicrobial, anti-inflammatory, anti-oxidant and hemolytic assays. Because of their unique physicochemical features, low cytotoxicity, excellent stability, exceptional antibacterial action, and significant interest in biomedical field. Various analytical techniques were used to assess the related phase constitution, elemental content, and surface morphology. The X-ray diffraction (XRD) patterns and field-emission scanning electron microscopy (FE-SEM) micrographs revealed that the Ru-Mn3O4 NFs had a tetragonal phase with a nanoflowers-like shape and Ru mainly existed as the metallic state. It has been found that Ru-Mn3O4 NFs hold higher microbial activities against various pathogens, making them ideal options for fighting bacterial infections.

Keywords: *Anti-oxidant, Hemolysis, Medicine, Nanotechnology, Novel Technique, Public Health Care.*

Introduction

In recent years, manganese-based nanomaterials (MnO_2 or Mn_3O_4) a critical raw material in a number of applications including sensors, energy storage, photocatalysis, pharmaceuticals, therapeutic systems, and biological applications [1]. Owing to their inherent divergence in redox properties, morphology, crystalline structure, surface architectures, excellent biocompatibility, and low toxicity [2]. Mn_3O_4 is present in trace amounts in a number of tissues and organs, including the pituitary, pancreas, liver, intestinal mucosa, and bones. It is essential for numerous biological processes, including those involving enzyme cofactors and nerve conduction and release controllers [3]. In addition, Mn_3O_4 nanomaterials have gained a lot of attention as bactericidal agents and brought up a new way of dealing with antibiotic-resistant bacteria. This is because nanomaterials can penetrate through nanopores in the millimeter range of cell membranes and release poisonous O_2* radicals to mutilate microbe cell membranes, resulting in an efficient limitation of microbial growth [4]. The biomedical, pharmaceutical, and drug delivery industries are paying increased attention to surface modification on Mn_3O_4 due to its magnetic behaviour, biocompatibility, and revolutionary features. For instance, Sukhdev et al. [5] evaluated the bioactivity properties of Mn_3O_4 NPs is a suitable material for antibacterial investigations. Likewise, Shaik et al [6] reported that Mn_3O_4 NPs are employed as antimicrobial and anticancer activity against A549 and MCF-7 cell lines.

It is a significant low-cost semiconductor material and visible light driven photocatalysis

Received: 20.02.2024 ***Accepted: 21.03.2024*** ***Published on: 29.04.2024***
****Corresponding Authors: vishnupriya@saveetha.com; veerakumarp.sdc@saveetha.com***

with a small band gap (~2.10 eV) which has prospective of industrial applications [7]. In particular, a strong oxidation behaviour and a wide range of oxidation numbers (+2, +3, +4) result in the production of different crystal structures and stoichiometry (MnO, MnO_2, Mn_2O_3, and Mn_3O_4), which is an essential constituent of metabolism and well regulated in biological systems [8]. Various methodologies have been developed to synthesize Mn_3O_4 NPs such as nanospheres (NSs), nanorods (NRs), nanowires (NWs), nanoflowers (NFs), nanoplates (NPLs), and nanourchins (NUs) have been widely explored for sustainable applications.

However, because to their magnetic behaviour, biocompatibility, and revolutionary features, surface modification of these nanoparticles is receiving increased interest in the biomedical, pharmaceutical, and drug delivery sectors [9]. Antibiotics are commonly utilized across veterinary and human healthcare due to their strong antimicrobial qualities and reasonable cost. But mishandling or overuse can cause them to build up in the body or from food, which may result in harmful effects on the well-being of the public such as cytotoxicity, nephrotoxicity, allergic reactions, and bacterial resistance. [10]. Thus, it is essential to develop a simple, sensitive, quick, and selective analytical method for tracking the amounts of antibiotics in food and the human body. In recent years, Mn_3O_4 NPs have been collected for antibacterial, and anti-fungal actions, and a great agreement of interest as one of the important possible therapeutic drugs against cancer.

Ru-based nanomaterials have grown in interest recently because of their unique redox, chemical, and physical characteristics, among others. In the field of biological sciences, they have demonstrated significant and effective antifungal and antioxidant properties [11]. For instance, Gopinath et al [12]. reported plant (*Gloriosa superba*) extract-mediated synthesis of Ru NPs and exhibited good antibacterial performance against gram-positive and gram-negative bacterial strains using standard disc diffusion method. In addition to being surface active, Ru NPs can release metal ions that are bioactive within biological systems. Thus, the anticancer activity of Ru NPs can be attributed to their enhanced affinity towards cancerous cells as compared to normal cells. As a result, their mode of action is twofold: similar to Fe, Ru binds more frequently to carcinogenic proteins. The anticancer effect of these Ru NPs may also be attributable to their capacity to bind DNA like cisplatin [13].

In this work, to synthesize Ru-Mn_3O_4 NFs architecture based on MW-HT approach has been presented. The as-prepared nanomaterial was characterized by X-ray diffraction (XRD), Fourier transform infrared spectrum (FT-IR), and field emission scanning electron microscopy-energy dispersive analysis (SEM-EDS) technique. The as-prepared Ru-Mn_3O_4 NFs were investigated for their biological activities, which included hemolytic, anti-microbial, anti-inflammatory, and antioxidant assay actions.

Materials and Methods

Chemicals and Reagents

Ruthenium(III) chloride trihydrate ($RuCl_3 \cdot 3H_2O$. 98%), manganese(II) chloride tetrahydrate ($MnCl_2$. $4H_2O$, ACS reagent, ≥98%), cetyltrimethylammonium bromide ($C_{16}H_{33}N(CH_3)_3Br$, CTAB, ≥98%), liquid ammonia (liq. NH_3, 28-30%), 2,2-diphenyl-1-picrylhydrazyl (DPPH), and phosphate-buffered saline (PBS, 0.05% TWEEN® 20, pH 7.4) were procured from the Sigma-Aldrich chemical company (Burlington, Massachusetts, United States). *Escherichia coli* (*E. coli*, ATCC 25922™), *Klebsiella pneumoniae* (*K. pneumoniae*, ATCC 13883™), *Staphylococcus aureus (S. aureus*, ATCC 25923™), *Candida albicans* (*C. albicans* ATCC 14053™) microorganisms were obtained from American Type Culture Collection. All other chemicals were used with analytical purity in the

experiment, and Milli-Q water was used throughout the work.

Preparation of Ru-Mn_3O_4 NFs

In a typical synthesis, ~50 mg of Ru(III), ~500 mg of Mn(II), and ~200 mg CTAB were mixed in 50 mL DI water. Then, the pH value of solution was adjusted to 8 using liq. NH_3 (20 mL) under rapid stirring (~1000 rpm) in a light red solution. The whole mixture was transferred into a 50 mL high-pressure Teflon-lined vessel and subjected to heating up to 180 ˚C for 6 h. When the reaction was completed, the autoclave could naturally drop to room temperature, and the final products were collected, rinsed three times with MilliQ water, and then dried at 80 °C for overnight. The sample was later calcined at 300 ˚C for 2 h. The overall preparation procedure for Ru-Mn_3O_4 MFs, as illustrated in Figure 1.

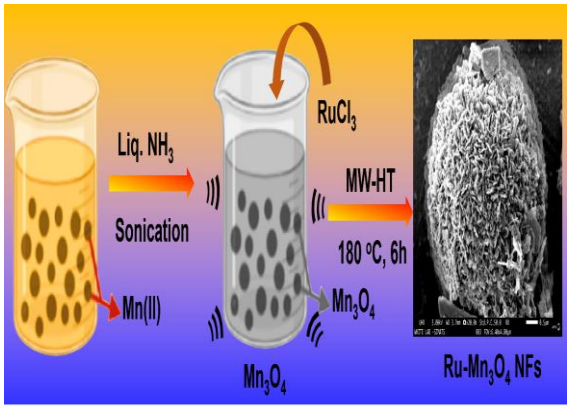

Figure 1: The Preparation of Ru-Mn_3O_4 NFs by the MW-HT Process.

Characterization

The XRD pattern of Ru-Mn_3O_4 MFs was examined using an X-ray diffractometer of typical Cu-K radiation at a scan rate of 0.05˚/min in the 20-90˚ range. An FT-IR spectrum was recorded in attenuated total reflectance (ATR) mode with a Bruker IR spectrometer (Billerica, Massachusetts, United States) in the region 4000-500 cm^{-1}. The surface morphology was examined using scanning electron microscopy (JEOL JSM-IT800 SEM, Tokyo, Japan) and energy EDS with the JSM-IT800 SEM apparatus equipped with a silicon drift detector (Oxford XMaxN 50 mm^2, Oxford Instruments, Abingdon, Oxfordshire, United Kingdom).

Antioxidant Activity

It is a rapid and popular test for determining the anti-radical activity of nanomaterials, expressed as IC_{50}, which denotes the concentration of each sample required to scavenge 50% of DPPH free radicals using ascorbic acid as a reference. DPPH is a typical nitrogen-concentrated free radical that is frequently employed to lessen the compound or vegetation extraction process's intense scavenger function. When hydrogen or electrons are accepted, the standard DPPH intensity is reduced. The DPPH assay is based on measuring the antioxidant capacity of Ru-Mn_3O_4 NFs to scavenge the DPPH radical. The reduced activity of the samples was determined by altering the color of the DPPH solution from blue/purple to yellow [14]. Typically, 2.0 mL of an alcoholic solution containing 0.1 mM DPPH was combined with 1.0 mL of different Ru-Mn_3O_4 NFs concentrations. The obtained whole mixture was incubated in the dark condition at least for 20 min\ at room temperature. The absorbance is measured at 517 nm against a control consisting of 1.0 mL DPPH in methanol. The percentage of DPPH radical scavenging activity was calculated using the following formula (1):

$$RSA(\%) = (A_{control} - A_{sample})/(A_{control}) \times 100 \quad (1)$$

where $A_{control}$ is the absorbance of DPPH without sample and A_{sample} is the absorbance of DPPH with the sample.

Antimicrobial Activity

The as-prepared Ru-Mn_3O_4 NFs were evaluated for their ability to inhibit the growth of pathogens like *E. coli, K. pneumonia, S. aureus,* and *C. albicans* using the Agar well diffusion method. Here, dimethyl sulfoxide (DMSO) was used to suspend nanomaterials at a concentration of 100 g/mL. Then, 25 and 100 mL of the Ru-Mn_3O_4 NFs were added to each well and the mixture was incubated for 18-24 hours at 37 °C. The standard antibiotic discs of ampicillin, chloramphenicol, gentamicin, and fluconazole were used as positive controls for *E. coli, K. pneumonia, S. aureus,* and *C. albicans*, respectively. After an overnight of incubation, the zone of inhibition in diameter was measured.

Hemolytic Activity

Hemolysis refers to the release of haemoglobin into the plasma because of the erythrocyte membrane being damaged. Khan et al. [15] approach was slightly modified to conduct the hemolysis activity test against nanomaterials. Typically, 1.0 mL of 3.8% sodium citrate was added to 9.0 mL of the blood sample to prevent blood clotting. It was then centrifuged in a centrifuge tube for five minutes at 3000 rpm. The pellet containing RBCs was re-suspended in 10 mL of PBS at a pH of 7.4 and the supernatant containing platelet poor plasma was discarded. he prepared Ru-Mn_3O_4 NFs were loaded with different concentrations (12.5, 25, 50, 100, and 200 g/mL) in five test tubes, then, each test tube was gently inverted after receiving 2 mL of erythrocyte suspension. After that, the tubes were gently shaken to maintain blood contact with the nanoparticle and incubated for 90 minutes at 37 °C. The same volume of erythrocyte solution was added to Triton X-100 and PBS (pH 7.4), respectively, to create positive and negative controls. After incubation, the samples were centrifuged for five minutes at 3000 rpm to remove the RBC cells. The supernatant was then carefully separated out and used for absorption studies at 540 nm using a UV-vis spectrophotometer against a PBS blank solution. The percentage of hemolytic index (%) was calculated by using the following formula (2):

$$Hemolysis(\%) = \frac{(A_s - A_o)}{A_{s+} - A_o} \times 100 \quad (2)$$

Here A_s, A_+ and A_o represent absorbance of RBCs treated with Ru-Mn_3O_4 NFs, absorbance of positive control and absorbance of negative control, respectively.

Anti-inflammatory Assay

The procedure used in this study was adapted from other previously reported studies [16,17]. The anti-inflammatory potentials of Ru-Mn_3O_4 NFs were examined through Bovine serum albumin (BSA) denaturation assay study. In this procedure, 50 µL of the Ru-Mn_3O_4 NFs was diluted with 450 µL of 5% weight/volume of BSA protein before being incubated at 37 °C for 20 minutes and then heated at 60 °C for 3 minutes. The percentage of inhibition was calculated with the following formula (3):

$$Inhibition(\%) = \left[\frac{V_t}{V_c} - 1\right] \times 100 \quad (3)$$

where, V_t = the absorbance of the test sample (Ru-Mn_3O_4 NFs and diclofenac) and V_c = absorbance of the control.

Statistical Analysis

Each experiment was carried out three times and was set up using a completely random block design. The results are shown as the mean and SD. GraphPad Prism 5 (version 6, Dotmatics, Boston, Massachusetts, United States) was used to do the statistical analysis. The one-way analysis of variance (ANOVA) Dunnett's multiple comparison test's p-value ($p < 0.05$) was used to determine the significance of the experiment.

Results

The construction of Ru-Mn_3O_4 NFs signifies one of the best nanomaterials in the pharmaceuticals field for biomedical applications. During the typical process, Ru-Mn_3O_4 NFs was synthesized by MW-HT method where Ru NPs were doped on Mn_3O_4 NFs. The MW-HT technique is a rapid and simple way to scale up nanomaterials with a flower-like structure. The HT technique and surfactant (CTAB) can be used in this process; the CTAB simultaneously serves as the structure-directing agent. The MW-HT synthesis approach not only makes rapid heating of the reaction medium possible but also significantly reduces the reaction time during the whole procedure. The possible Ru-Mn_3O_4 NFs was synthesized utilizing Ru(III), Mn(II) salts and liq. NH_3 solution. The possible reactions are shown in Equations (4-6).

$$NH_4OH \overset{MW-HT}{\rightarrow} NH_4^+ + (OH)^-_{(aq)} \quad (4)$$

$$6Mn^{2+} + 12(OH)^-_{(aq)} + O_2 \overset{MW-HT}{\rightarrow} 2Mn_3O_4 + 6H_2O \quad (5)$$

$$Ru(III) + Mn_3O_4 \overset{MW-HT}{\rightarrow} Ru(0) - Mn_3O_4 \quad (6)$$

The structure of Ru-Mn_3O_4 NFs is characterized by XRD, which is presented in Figure 2a. It exhibited a single phase hexagonal wurtzite structure that well matched with JCPDS values (JCPDS Card No. 24-0734). The sharp diffraction peaks are indicating the hausmannite crystal phase which is in good agreement with previous report [18]. In addition, there are no other diffraction peaks of any other impurities was observed demonstrating high crystalline quality. The Ru-Mn_3O_4 NFs is also analyzed by FT-IR spectroscopy in the range of ~4000–400 cm^{-1} (Figure 2b). The absorption band at ~3416 cm^{-1} is attributed to O-H stretching mode and the absorption peak exists near around 1644 and 1384 cm^{-1} could be attributed to O-H bending vibration combined with Mn atoms. The characteristic of Mn–O has both stretching modes (~630–650 cm^{-1}) in tetrahedral sites and distortion vibration (525–560 cm^{-1}) in an octahedral environment. Typically, Ru-Mn_3O_4 NFs have three standard significant bands ~552, 723, and 756 cm^{-1}, these bands correspond to the vibration of manganese species (Mn^{3+}) at an octahedral site [19].

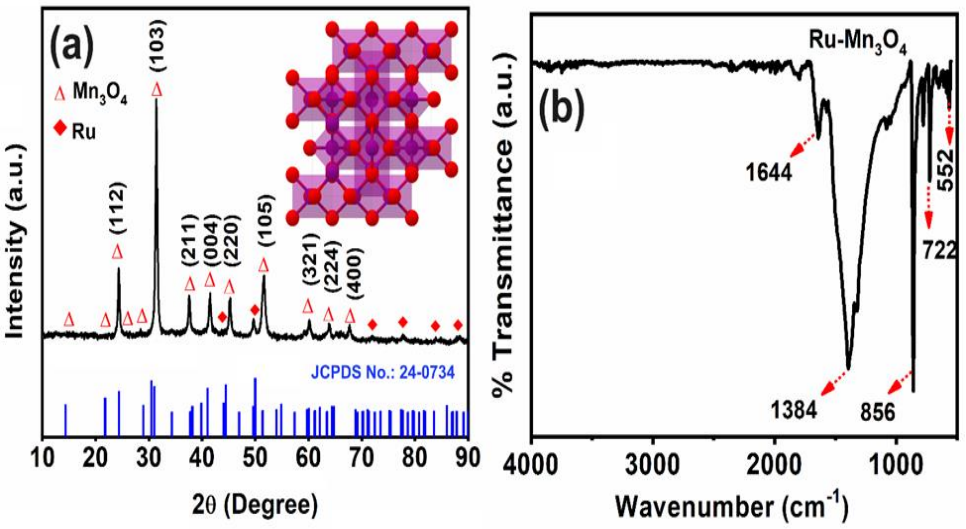

Figure 2. (a) X-ray Diffraction Pattern and (b) Fourier Transform Infrared Spectrum of the Ru-Mn_3O_4 NFs. JCPDS: Joint Committee on Powder Diffraction Standards.

The morphology of the Ru-Mn_3O_4 NFs was analyzed by FE-SEM and exhibit a flower-like morphology (see Figures 3a-3c). In the meantime, it was evident that they had great densities and primarily had sizes of 300–500 nm. It contains several NPs approximate to

spherical shaped formed at nanoscale range with an average size of 50 nm. The EDS spectra show peaks relevant to Ru, Mn, and oxygen (O) signals, confirming the formation of Ru-Mn_3O_4 NFs (Figure 3d). The carbon signal emitted by the carbon tape is noticeable. The quantities of Ru, Mn, and O elements are evaluated from the corresponding EDS analysis (Figure 3d inset), confirming that the Ru-Mn_3O_4 NFs are composed of only Ru, Mn, and O elements.

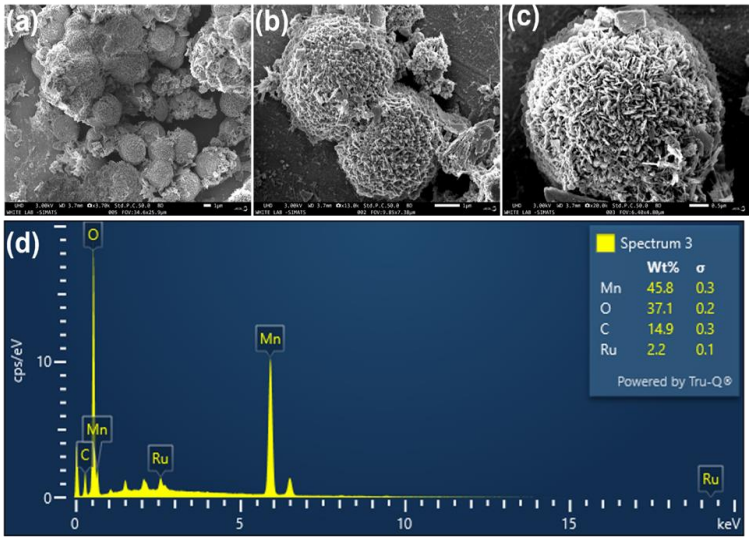

Figure 3. (a-b) Field Emission Scanning Electron Microscope Images and (c) Energy Dispersive X-ray Spectroscopy Spectrum of the Ru-Mn_3O_4 NFs.

Antimicrobial Activity

The Ru-Mn_3O_4 NFs antimicrobial action was observed against the predominant opportunistic human pathogens such as *E. coli*, *K. pneumonia*, *S. aureus*, and *C. albicans*; the corresponding ampicillin, chloramphenicol, gentamicin, and fluconazole were used as reference drugs and to compare the efficacy of Ru-Mn_3O_4 NFs antibacterial properties. We tested anti-bacterial activity in a dose-dependent manner using the Ru-Mn_3O_4 NFs, as displayed in Figure 4. The antibacterial activity was very low (<1 mm) against *E. coli* (Gram-negative), *K. pneumonia* (Gram-negative), *S. aureus* (Gram-positive), and *C. albicans*. (i.e., minimum zone of inhibition was observed at a concentration of 25 µg/mL. In the case of 100 µg/mL, 13 ± 0.3, 17 ± 0.4, 26 ± 0.3, and 15 ± 0.2 were observed for the *E. coli*, *K. pneumonia*, *S. aureus*, and *C. albicans*. The maximum antibacterial activity was observed in Gram-negative (*K. pneumonia*) and Gram-positive (*S. aureus*). This is due to the size of the particles arranged at NFs and it possesses unique properties. Figure 4 represents a selective mechanism of Ru-Mn_3O_4 NFs that depends on the Ru concentration and the type of cell membrane structure according to the microbiological properties of specific bacterial strains. At the application of a higher concentration of Ru-Mn_3O_4 NFs (100 µg/mL), a greater bactericidal effect of Ru-Mn_3O_4 NFs was observed when compared to 25 µg/mL. The reason for growth inhibition can be the possible interaction between the external membrane of bacteria and the Ru-Mn_3O_4 NFs. It may disrupt the integrity of cell membranes causing malfunctioning of enzymes and increasing cell permeability leading to bacterial cell death [20,21]. Also, Ru-Mn_3O_4 NFs exhibit stronger anti-bacterial activity against the studied bacterial strains because of their excellent stability in the growing medium, which promotes more interactions between bacterium and Ru-Mn_3O_4 NFs. The results indicate that the as-prepared Ru-Mn_3O_4 NFs is

a favorable contender for usage pharmaceutical industries and food packaging applications.

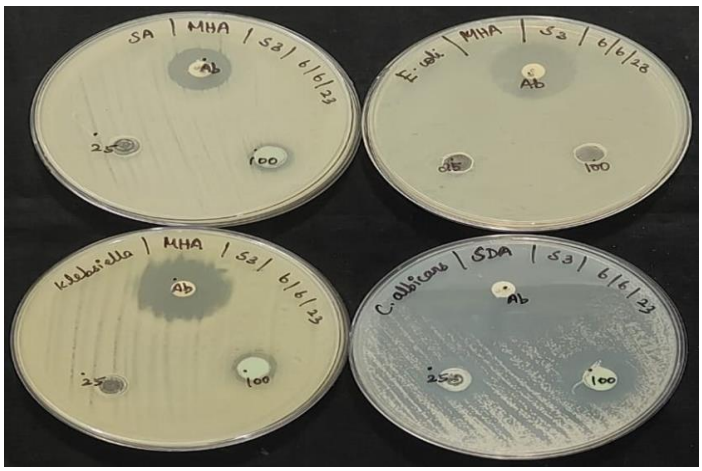

Figure 4. The Antimicrobial Activity of Ru-Mn_3O_4 NFs Against Various Pathogens: *Escherichia coli (E. coli), Klebsiella pneumonia (K. pneumonia), Staphylococcus aureus (S. aureus),* and *Candida albicans (C. albicans).*

Antioxidant Activity

The DPPH scavenging activity of Ru-Mn_3O_4 NFs is shown in Figure 5. The potential of ascorbic acid (AA) to scavenge DPPH radicals is directly proportional to the concentrations. DPPH radical scavenging activity of Ru-Mn_3O_4 NFs and standard AA is presented in Figure 5. The cumulative effect of Ru-Mn_3O_4 NFs shows maximum efficiency, which is $57.28 \pm 0.15\%$, $60.84 \pm 0.11\%$, $70.62 \pm 0.12\%$, $74.51 \pm 0.12\%$, and $78.82 \pm 0.15\%$ in DPPH radical scavenging activity at 100 µg/mL, whereas the standard AA exhibit $80.58 \pm 0.15\%$ activity. The inhibition of DPPH activity assumes the existence of a linear relationship (with should also be validated) between DPPH activity and Ru-Mn_3O_4 NFs concentration (Figure 5) the relationship could be magnified by coefficient correlation and also be tested by p-value and it was compared with AA [22].

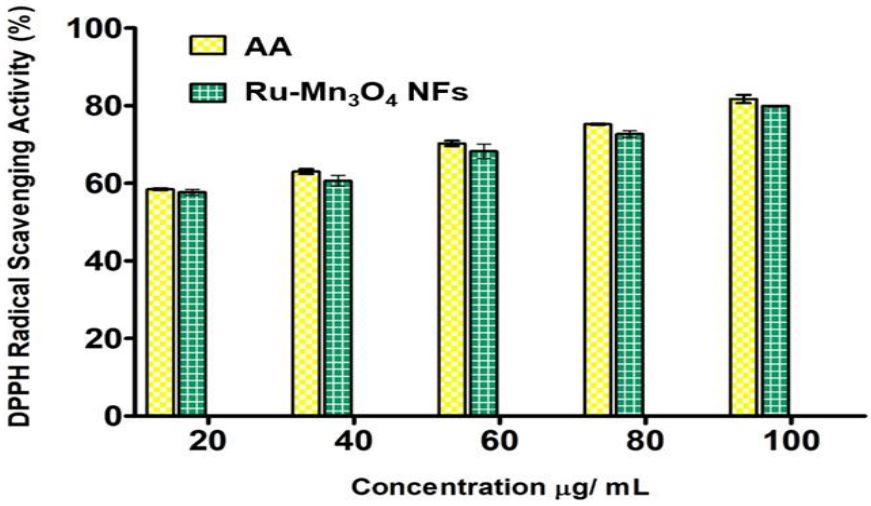

Figure 5. The Antioxidant Property of Ru-Mn_3O_4 NFs Using DPPH Radical Scavenging Potential with Different Concentrations (n = 3). The Experiment was Performed in Triplicates and Values are Expressed in mean ± SD. *Values are Statistically Significant from the Group Incubated ($P < 0.05$).

Anti-inflammatory Assay

Inflammation is caused by cellular and tissue damage resulting from an imbalance between

the regulatory signals of the inflammatory process, which leads to the development of cancer [23]. In this study, a dose-dependent activity profile at the concentration range of 25 to 400 µg/mL was observed for the Ru-Mn_3O_4 NFs and the used standard drug of diclofenac, as shown in the histogram plot (see Figure 6). The standard diclofenac drug showed better activity in all the used concentrations than the prepared Ru-Mn_3O_4 NFs. However, at 400 µg/mL, the percentage inhibition was near close. Furthermore, the maximum inhibitory percentage of 80.54 and 88.21% were observed at the highest concentration of 25-400 µg/mL for the Ru-Mn_3O_4 NFs and diclofenac, respectively. The experiment was performed in triplicates and values are expressed in mean ± SD. This shows that the Ru-Mn3O4 NFs may reduce inflammation and help develop new anti-inflammatory drugs [24].

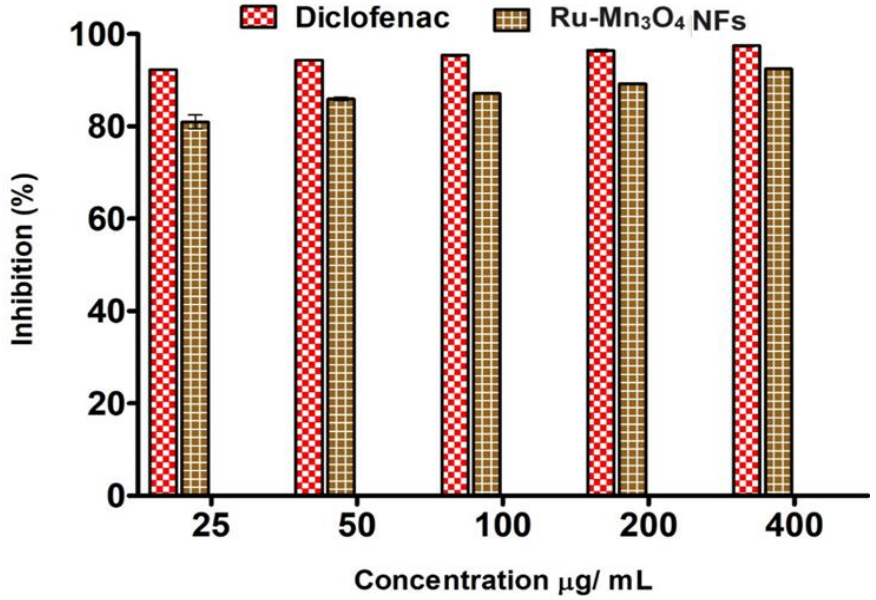

Figure 6. Anti-inflammatory Activity of Ru-Mn_3O_4 NFs. The Experiment was Performed in Triplicates and Values are Expressed in mean ± SD. *Values are Statistically Significant Between Different Concentrations ($P < 0.05$).

Hemolytic Assay

To estimate the possible hemolysis, a biocompatibility assay was conducted to verify the toxicity of Ru-Mn_3O_4 NFs on RBCs. The results of biocompatibility assay with Ru-Mn_3O_4 NFs were showed less hemolysis with respect to positive control (Figure 7). The less toxic nature of Ru-Mn_3O_4 NFs was observed through in-vitro analysis which showed their reliability and suitability in biomedical sciences [25]. The graph was illustrated the percentage of hemolysis in Ru-Mn_3O_4 NFs treated samples with positive control. In comparison to the control, the Ru-Mn_3O_4 NFs demonstrated less than 5% hemolysis in erythrocytes at a lower concentration of 12.5 µg/mL. The hemolytic assay test results are shown in Figure 7. However, hemolysis increased as a function of increasing the concentrations of Ru-Mn_3O_4 NFs from 25, 50, 100, and 200 µg/mL. The results illustrated the dose-dependent raising protective action of Ru-Mn_3O_4 NFs with a gradual increase in the concentration from 25 to 200 µg/mL. These encouraging results of Ru-Mn_3O_4 NFs with significant protective action intern low hemolysis percentage show the manifestation of hemocompatibility of Ru-Mn_3O_4 NFs towards human RBCs [26].

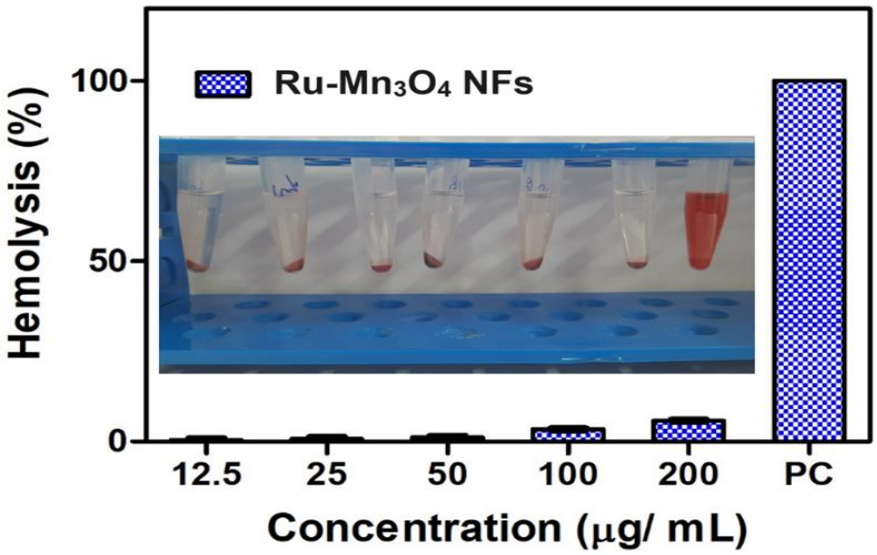

Figure 7. Hemolytic Activity of Ru-Mn_3O_4 NFs. The Experiment was Performed in Triplicates, and it was Expressed as Mean ± Standard Deviation (SD). *Values are Statistically Significant Compared to the Control Group ($P<0.05$).

Discussion

In this present work, the XRD diffractions plane (112), (103), (211), (004), (220), (105), (321), (224), and (400) at 2θ = 29.1º, 32.5º, 36.3º, 38.2º, 44.6º, 50.8º, 58.7º, 60.0º, and 64.8 º, respectively represented the tetragonal phase and matched with JCPDS card no. 24–0734 (Figure 2a). It exhibited tetragonal structure (hausmannite, I41/amd) with constant lattice values 'a' = 0.5746 nm and 'c' = 0.9463 nm. This study shows that the Ru-Mn_3O_4 NFs are tetragonal with crystalline in nature and the average crystallite size is estimated by Scherrer's equation [27] from the full-width-half-maximum of the (110) peak of the XRD pattern. Based on the above Scherrer's equation, the average crystalline size is ~50 nm ± 5 nm. The FT-IR absorption peaks revealed the vibrational modes of Ru-Mn_3O_4 NFs in the range 700-400 cm^{-1} with stretching of Mn-O, which shows that the metal oxide peak suggests the formation of the Mn_3O_4 nanocrystals (Figure 2b). It should be note that most of the Ru-Mn_3O_4 NFs in the FE-SEM images were found to be flower-like morphology and uniformly dispersed in nature. Notably, these nanostructures have rough surface and large number of voids (Figure 2c). The EDS spectrum for the Ru-Mn_3O_4 NFs confirmed Ru, Mn, and O in the Ru-Mn_3O_4 NFs with no impurity peaks (Figure 2d). The Ru-Mn_3O_4 NFs were exploited for hemolytic assay, anti-microbial, anti-inflammatory, and antioxidant activities, owing to the doping of Ru, large surface-to-volume ratio, excellent redox behaviour, and remarkable biocompatibility [28]. The antibacterial activity of the synthesized Ru-Mn_3O_4 NFs against the Gram-negative (*K. pneumonia*) and Gram-positive (*S. aureus*) pathogens were observed, with the maximum ZOI, shown in Figure 4. The same type of highest-growth inhibitory result was reported in Gram-negative and Gram-positive pathogens by Pazos-Ortiz et al [29]. The Ru-Mn_3O_4 NFs have a large surface area, redox behaviour making them highly reactive. Doping of Ru to the metal oxide matrix has been demonstrated to improve physical, chemical and bactericidal properties of metal oxides. The distinctively high surface-to-volume ratio of Ru-Mn_3O_4 NFs permits them to interact with the cell membrane of the bacteria through their surface, resulting in the death of the bacteria. Notably, with an increased DPPH radical impact, it is stated that MW-HT

synthesized Ru-Mn_3O_4 NFs have more antioxidant properties, are non-toxic, and are environmentally friendly, as well as they are a prospective candidate for a variety of medicinal applications [30]. Another study employed Ru-Mn_3O_4 NFs to assess protein denaturation in comparison to the nonsteroidal inflammatory drug diclofenac. The protein denaturation experiment results indicate that it helps break down proteins, which gives it anti-inflammatory features. For Ru-Mn3O4 NFs, the range of protein denaturation inhibition is 80.54 and 88.21% at doses between 25 and 400 µg/mL (Figure 6). This outcome is comparable to the anti-inflammatory properties of diclofenac (94%) and metformin (85.9%) used to treat diabetes. Navada et al. [31] reported for phytofunctionalized CuO NPs demonstrated anti-inflammatory study with inhibitory potential of 67-92%. Similarly, ZnO NPs synthesized from a mixture of clove buds and cinnamon bark sticks were found to have a 91.1% anti-inflammatory activity [32]. Therefore, our findings provide a viable foundation for mitigating inflammation and protein breakdown in hyperglycemic situations. As shown in Figure 6, at all concentrations of Ru-Mn_3O_4 NFs, except at 25 µg/mL, hemolysis is below the 5% allowed by the International Organization for Standardization (ISO) 10993-4 [33]; therefore, concentrations below 25 µg/mL (Figure 7) can be considered hemocompatible. Based on these findings, it can be concluded that Ru-Mn_3O_4 NFs have promising uses in biomedicine and other biological processes.

Recently, there have been efforts by researchers to modify the morphology or size of Ru-Mn_3O_4 NFs to enhance biological activity. We could attempt a plethora of additional combinations. Additionally, metal doped Mn_3O_4-based nanocomposites have become a viable option for obtaining enhanced and sustainable biological properties. [34-37] The biological performance translates into more active sites, adaptability, and selectivity as a result of the synergistic effects. Therefore, more research in these fields is required to demonstrate the potential production and use of Mn_3O_4-based biological activities in modern drug discovery. Finally, we think that further study is required to assess and possibly even relate the structure of the modifying material containing Ru-Mn_3O_4 NFs to the anticipated future performance of the developed biomedical studies.

Novelty of the Work

Various metal oxide-based nanomaterials, including cobalt oxide (Co_3O_4), nickel oxide (NiO), copper oxide (Cu_2O), and zinc oxide (ZnO) have been used in biomedical applications due to their high electrical conductivity, redox behaviour, large surface area-to-volume ratio, and biocompatibility. On the other hand, Mn_3O_4 also offers many benefits over other transition nanomaterials, including low cost and being an essential trace metal in the human body that is mostly absorbed in the stomach and small intestine before being eliminated in the bile. Additionally, it plays a significant catalytic role and regulates many enzymes and proteins in the body through multiple mechanisms. The MW-HT approach is one of the most well-known and widely employed methods for the synthesis of diverse Mn_3O_4 nanostructured materials, including Ru-Mn_3O_4 NFs. This method is simple, cost-effective, eco-friendly, and easily controllable. These characteristics make it highly advantageous for the large-scale synthesis of Ru-Mn_3O_4 NFs. Herein, the Ru-Mn_3O_4 NFs were prepared by the MW-HT method and characterized with different sophisticated analytical tools and used for applications. The Ru-Mn_3O_4 NFs so prepared were utilized for anti-microbial, antioxidant, anti-inflammatory, and anti-hemolytic activities.

Limitation

This study explored the application of Ru-Mn_3O_4 NFs and addressed several biomedical

functions with encouraging outcomes in laboratory-based practical studies. However, additional research is required to transition from controlled laboratory settings to practical, real-world scenarios. While most of our present research has been on immediate consequences, there is clearly a need to examine long-term impacts, considering the possibility of bioaccumulation. Another limitation is that a single antibiotic is chosen as a reference. Although hemolytic activity has been evaluated, the future research path has to include a more thorough cytocompatibility assessment that considers unintended consequences, the dosage of Ru-Mn_3O_4 NFs, and turning the form stability. Moreover, a thorough analysis of Ru-Mn_3O_4 NFs interactions with bioenvironments and adherence to regulatory requirements give a route for future research in medicine. Further studies need to be performed in natural conditions (in vitro or in vivo) to find the actual mechanism of Ru-Mn_3O_4 NFs in reducing inflammation. However, it is important to search for efficient Ru-Mn_3O_4 NFs, to use low concentrations for safety, and also to explore their cytotoxicity in different mammalian cell lines.

Conclusions

In summary, we were able to effectively create the Ru-Mn_3O_4 NFs using an easy-to-afford MW-HT method. The Ru-Mn_3O_4 NFs were characterized using XRD, FT-IR, and FE-SEM-EDS methods. The morphology of the nanoflowers was confirmed by FE-SEM microscopy, while the XRD pattern revealed a tetragonal structure. We tested the antimicrobial activities using Ru-Mn_3O_4 NFs through the agar disk-diffusion method, and the results were more effective. Notably, the hemolytic assay revealed that Ru-Mn_3O_4 NFs is compatible with low doses and have the potential to be well-tolerated in therapies. In addition, the antioxidant and anti-inflammatory activity results showed that the Ru-Mn_3O_4 NFs perform better when compared to the standard. Moreover, Ru-Mn_3O_4 NFs can be exploited as a biocompatible nanomaterial in the fields of biomedicine, pharmaceuticals, nutrition, agriculture, and the environment because of their favorable antifungal activity.

Author Contributions

All authors have reviewed the final version to be published and agreed to be accountable for all aspects of the work. Concept and design: Pitchaimani Veerakumar, Vishnu Priya Veeraraghavan, Hooriyah Laiq Ahmed Khan Acquisition, analysis, or interpretation of data: Pitchaimani Veerakumar, Vishnu Priya Veeraraghavan, Hooriyah Laiq Ahmed Khan Drafting of the manuscript: Pitchaimani Veerakumar, Vishnu Priya Veeraraghavan, Hooriyah Laiq Ahmed Khan Critical review of the manuscript for important intellectual content: Pitchaimani Veerakumar, Vishnu Priya Veeraraghavan, Hooriyah Laiq Ahmed Khan Supervision: Pitchaimani Veerakumar, Vishnu Priya Veeraraghavan

Disclosures

Human subjects: All authors have confirmed that this study did not involve human participants or tissue. Animal subjects: All authors have confirmed that this study did not involve animal subjects or tissue. Conflicts of interest: In compliance with the ICMJE uniform disclosure form, all authors declare the following: Payment/services info: All authors have declared that no financial support was received from any organization for the submitted work. Financial relationships: All authors have declared that they have no financial relationships at present or within the previous three years with any organizations that might have an interest in the submitted work. Other relationships: All authors have declared that there are no other relationships or activities that could appear to have influenced the submitted work.

Acknowledgements

The authors would like to express their profound gratitude to Saveetha Dental College and Hospitals, Saveetha Institute of Medical and Technical Sciences, Chennai, for their unwavering support toward the successful completion of this study.

Declaration of Competing Interest

The authors declare that they have no known competing financial interests or personal relationships that could have appeared to influence the work reported in this paper.

References

[1] Beknalkar, S. A., Teli, A. M., Bhat, T. S., Pawar, K. K., Patil, S. S., Harale, N. S., Shin, J. C., Patil, P. S., 2022, Mn_3O_4 based materials for electrochemical supercapacitors: Basic principles, charge storage mechanism, progress, and perspectives. Journal of Materials Science & Technology 130, 227-248.

[2] Jain, P., Jangid, A.K., Kulhari, D.P. and Kulhari, H., 2024, Designing of manganese-based nanomaterials for pharmaceutical and biomedical applications. Journal of Materials Chemistry B. 12, 577-608.

[3] Ding, B., Zheng, P., Ma, P. A., Lin, J., 2020, Manganese oxide nanomaterials: synthesis, properties, and theranostic applications. Advanced Materials, 32, 1905823.

[4] Spiro, T. G, Bargar, J. R, Sposito, G., Tebo, B. M., 2010, Bacteriogenic manganese oxides. Accounts of Chemical Research., 43, 2-9.

[5] Sukhdev, A., Challa, M., Narayani, L., Manjunatha, A. S., Deepthi, P. R., Angadi, J. V., Kumar, P. M., Pasha, M., 2020, Synthesis, phase transformation, and morphology of hausmannite Mn3O4 nanoparticles: photocatalytic and antibacterial investigations. Heliyon, 6, e03245.

[6] Shaik, M. R., Syed, R., Adil, S. F., Kuniyil, M., Khan, M., Alqahtani, M. S., Shaik, J. P., Siddiqui, M. R. H., Al-Warthan, A., Sharaf, M. A., Abdelgawad, A., 2021, Mn3O4 nanoparticles: Synthesis, characterization and their antimicrobial and anticancer activity against A549 and MCF-7 cell lines. Saudi Journal of Biological Sciences, 28, 1196-1202.

[7] Bhattacharya, P., Swain, S., Giri, L., Neogi, S., 2019, Fabrication of magnesium oxide nanoparticles by solvent alteration and their bactericidal applications. Journal of Materials Chemistry B. 7, 4141–4152.

[8] Hoseinpour, V., Ghaemi, N., 2018, Green synthesis of manganese nanoparticles: Applications and future perspective—A review. Journal of Photochemistry Photobiology B Biology, 189, 234–243.

[9] Yadav, P., Bhaduri, A., Thakur, A., 2023, Manganese oxide nanoparticles: An insight into structure, synthesis and applications. Chemical and Biochemical Engineering Reviews 10, 510-528.

[10] Perachiselvi, M., Bagavathy, M. S., Samraj, J. J., Pushpalaksmi, E., Annadurai, G., 2020, Synthesis and characterization of Mn_3O_4 nanoparticles for biological studies. Applied Ecology Environmental Science, 8, 273-277.

[11] Gupta, P. K., Mishra, L., 2020, Ecofriendly ruthenium-containing nanomaterials: synthesis, characterization, electrochemistry, bioactivity and catalysis. Nanoscale Advances, 2,1774-1791.

[12] Gopinath, K., Karthika, V., Gowri, S., Senthilkumar, V., Kumaresan, S. and Arumugam, A., 2014, Antibacterial activity of ruthenium nanoparticles synthesized using Gloriosa superba L. leaf extract. Journal of Nanostructure in Chemistry, 4, 1-6.

[13] Anjum, S. M., Riazunnisa, K., 2022. Fine ultra-small ruthenium oxide nanoparticle synthesis by using Catharanthus roseus and Moringa oleifera leaf extracts and their efficacy towards in vitro assays, antimicrobial activity and catalytic: adsorption kinetic studies using methylene blue dye. Journal of Cluster Science, 33, 1103–1117.

[14] Pradeep, V., Veerakumar, P., Veeraraghavan, V. P. 2024, Facile microwave-assisted hydrothermal synthesis of copper oxide nanoneedle arrays for practical biomedical applications. Cureus, 16, e51678.

[15] Khan, S., Ansari, A. A., Khan, A. A., Abdulla, M., Al-Obeed, O., Ahmad, R., 2016, In vitro

evaluation of anticancer and biological activities of synthesized manganese oxide nanoparticles. Medicinal Chemistry Communications, 7, 1647-1653.

[16] Pandiyan, I., Sri, S. D., Indiran, M. A., Rathinavelu, P. K., Prabakar, J., Rajeshkumar, S., 2022, Antioxidant, anti-inflammatory activity of Thymus vulgaris-mediated selenium nanoparticles: An in vitro study. Journal of Conservative Dentistry, 25, 241.

[17] Adeyemi, J. O., Onwudiwe, D. C., Oyedeji, A.O., 2022, In vitro α-glucosidase enzyme inhibition and anti-inflammatory studies of Mn_3O_4 nanoparticles mediated using extract of Dalbergiella welwitschia. Results in Chemistry, 4, 100497.

[18] Liu, X., Chen, Z., Sun, H., Chen, L., Peng, Z. and Liu, Z., Investigation on Mn_3O_4 coated Ru nanoparticles for partial hydrogenation of benzene towards cyclohexene production using $ZnSO_4$, $MnSO_4$ and $FeSO_4$ as reaction additives. Nanomaterials, 2020, 10: 809.

[19] Perachiselvi, M., Bagavathy, M. S., Samraj, J. J., Pushpalaksmi, E., Annadurai, G., 2020, Synthesis and characterization of Mn_3O_4 nanoparticles for biological studies. Applied Ecololgy Environmental Sciences, 8, 273-277.

[20] Rajeshkumar, S., Lakshmi, T., Tharani, M., 2021, Green synthesis of copper nanoparticles synthesized using black tea and its antibacterial activity against oral pathogens. International Journal of Dentistry Oral Science 8, 4156-4159.

[21] Nasim, I., Kumar, S. R., Vishnupriya, V. Jabin, Z., 2020, Cytotoxicity and anti-microbial analysis of silver and graphene oxide bio nanoparticles. Bioinformation, 16, 831.

[22] Rajeshkumar, S., Sandhiya, D., 2020, Biomedical applications of zinc oxide nanoparticles synthesized using eco-friendly method. Nanoparticles and their biomedical applications, pp-65-93.

[23] Agarwal, H., Nakara, A., Shanmugam, V. K., 2019, Anti-inflammatory mechanism of various metal and metal oxide nanoparticles synthesized using plant extracts: A review. Biomedical Pharmacotherpy, 109, 2561–2572.

[24] Nasim, I., Rajeshkumar, S. and Vishnupriya, V., 2021, Green synthesis of reduced graphene oxide nanoparticles, its characterization and antimicrobial properties against common oral pathogens. International Journal of Dentistry Oral Science, 8, 1670-1675.

[25] Ibrahim, A., Hammadi, M., 2023, Green synthesis of Mn3O4 nanoparticles using chia seeds extract, characterization, and cytotoxicity on the HL-60 cells. History of Medicine, 9, 1537-1542.

[26] Nasim, I., Jabin, Z., Kumar, S. R., Vishnupriya, V., 2022, Green synthesis of calcium hydroxide-coated silver nanoparticles using Andrographis paniculata and Ocimum sanctum Linn. leaf extracts: An antimicrobial and cytotoxic activity. Journal Conservation Dentistry 25, 369.

[27] Prasad, A.S. Green synthesis of nanocrystalline manganese (II,III) oxide, 2017, Material Sciences. Semiconductor Process. 71, 342–347.

[28] Sharma, J. K., Srivastava, P., Ameen, S., Akhtar, M. S., Singh, G., Yadava, S., 2016, Azadirachta indica plant-assisted green synthesis of Mn3O4 nanoparticles: Excellent thermal catalytic performance and chemical sensing behavior, Journal of Colloid Interface Sciences. 472, 220–228.

[29] Pazos-Ortiz, E., Roque-Ruiz, J. H., Hinojos-Márquez, E. A., López-Esparza, J., Donohué-Cornejo, A., Cuevas-González, J. C., Espinosa-Cristóbal, L. F., Reyes-López, S. Y., Dose-dependent antimicrobial activity of silver nanoparticles on polycaprolactone fibers against gram-positive and gram-negative bacteria. Journal of Nanomaterials, 2017. Article ID 4752314.

[30] Kumar, G. S., Venkataramana, B., Reddy, S. A., Maseed, H., Nagireddy, R.R., 2020, Hydrothermal synthesis of Mn_3O_4 nanoparticles by evaluation of pH effect on particle size formation and its antibacterial activity. Advances in Natural Sciences: Nanoscience and Nanotechnology, 11, 035006.

[31] Navada, K. M., G. K, N., D'Souza, J. N., Kouser, S., D. J, M., 2021, Synthesis, characterization of phyto-functionalized CuO nano photocatalysts for mitigation of textile dyes in waste water purification, antioxidant, anti-inflammatory and anticancer evaluation. Applied Nanoscience, 11, 1313-1338.

[32] Mohapatra, S., Leelavathi, L., Rajeshkumar, S., Sakthi, D. S., Jayashri, P., 2020, Assessment of cytotoxicity, anti-inflammatory and antioxidant activity of zinc oxide nanoparticles synthesized using clove and cinnamon formulation-an In-vitro study. Journal of Evolution Medical Dental Science, 9, 1859-1865.

[33] Mansi, K., Kumar, R., Narula, D., Pandey, S. K., Kumar, V., Singh, K., 2022, Microwave-induced CuO nanorods: a comparative approach between curcumin, quercetin, and rutin to study their antioxidant, antimicrobial, and anticancer effects against normal skin cells and human breast cancer cell lines MCF-7 and T-47D. ACS Applied Bio Materials, 5, 5762-78.

[34] Ealla KKR, Veeraraghavan VP, Ravula NR, Durga CS, Ramani P, Sahu V, Poola PK, Patil S, Panta P (2022) Silk Hydrogel for Tissue Engineering: A Review. J Contemp Dent Pract 23:467–477

[35] Patil S, Sujatha G, Varadarajan S, Priya VV (2022) A bibliometric analysis of the published literature related to toothbrush as a source of DNA. World J Dent 13:S87–S95

[36] Ganesan A, Muthukrishnan A, Veeraraghavan V (2021) Effectiveness of Salivary Glucose in Diagnosing Gestational Diabetes Mellitus. Contemp Clin Dent 12:294–300

[37] Karthik EVG, Priya V (2021) Gayathri. R, Dhanraj Ganapathy. Health Benefits Of Annona Muricata-A Review. Int J Dentistry Oral Sci 8:2965–2967